Birefringent Stable Glass with Predominantly Isotropic Molecular Orientation

Tianyi Liu,[1] Annemarie L. Exarhos,[2] Ethan C. Alguire,[1] Feng Gao,[1] Elmira Salami-Ranjbaran,[1] Kevin Cheng,[1] Tiezheng Jia,[1] Joseph E. Subotnik,[1] Patrick J. Walsh,[1] James M. Kikkawa,[2] and Zahra Fakhraai[1,*]

[1]*Department of Chemistry, University of Pennsylvania, Philadelphia, Pennsylvania 19104, USA*

[2]*Department of Physics and Astronomy, University of Pennsylvania, Philadelphia, Pennsylvania 19104, USA*

(Received 1 March 2017; revised manuscript received 15 May 2017; published 31 August 2017)

Birefringence in stable glasses produced by physical vapor deposition often implies molecular alignment similar to liquid crystals. As such, it remains unclear whether these glasses share the same energy landscape as liquid-quenched glasses that have been aged for millions of years. Here, we produce stable glasses of 9-(3,5-di(naphthalen-1-yl)phenyl)anthracene molecules that retain three-dimensional shapes and do not preferentially align in a specific direction. Using a combination of angle- and polarization-dependent photoluminescence and ellipsometry experiments, we show that these stable glasses possess a predominantly isotropic molecular orientation while being optically birefringent. The intrinsic birefringence strongly correlates with increased density, showing that molecular ordering is not required to produce stable glasses or optical birefringence, and provides important insights into the process of stable glass formation via surface-mediated equilibration. To our knowledge, such novel amorphous packing has never been reported in the past.

DOI: 10.1103/PhysRevLett.119.095502

A metastable supercooled liquid (SCL) is formed by rapid quenching of a liquid to a temperature below its melting point. Further cooling slows down the SCL's dynamics until the system falls out of equilibrium at its glass transition temperature (T_g) [1,2]. Compared to their crystalline counterparts, glasses have lower density and reside at higher energy states. As such, when held at temperatures below T_g, properties of glasses such as density and enthalpy gradually evolve towards their corresponding SCL state. This mechanism is termed physical aging [3–8].

Physical aging is a slow process. Experiments on amber have shown that a 2% increase in density requires aging for millions of years [9,10]. Recent studies discovered that physical vapor deposition (PVD) at substrate temperatures just below T_g can yield glasses with properties similar to well-aged glasses in laboratory time scales. Compared to liquid-quenched glasses, these stable glasses have higher density (by ∼1.5%) [11,12] and lower heat capacity (by ∼4%) [13–15]. It has been suggested that surface-mediated equilibration (SME) during PVD provides a route to overcome kinetic barriers for rearrangement, and achieve these low-energy states within hours [16–22] as opposed to millions of years.

While most properties of stable glasses (SGs) resemble those of aged glasses, the emergence of optical birefringence at low deposition temperatures ($T_{dep} < 0.9T_g$) [23–30] implies significant differences between their packing arrangements. Optical birefringence is quantified as the difference between the out-of-plane and in-plane indices of refraction, with respect to the polarization of the electric field. As in liquid-crystalline systems, birefringence in PVD glasses has been interpreted as an indication of preferential molecular orientation induced by the substrate or the free surface. For molecules with large aspect ratios, the existence of molecular ordering has been supported by experiments [23–26,29,30] and simulations [28,31,32]. A liquid-crystal-linelike order implies that PVD films generated by SME do not share the same energy landscape as the SCL, and thus are unable to reveal properties of SCL at low temperatures.

However, SGs made of smaller and more isotropic molecules still show birefringence [11,33–35]. Other measures of structure such as wide angle x-ray scattering (WAXS) [36–39], Brillouin light scattering [33], and magnetic anisotropy [40] also indicate subtle differences between the in-plane and out-of-plane structure factor and therefore the pair correlation functions. The above differences cannot be solely explained by molecular orientation. Furthermore, sputtered metallic glasses, which are by default made of isotropic constituents can still access a higher stability state upon vapor deposition [41]. Therefore, it is crucial to question whether molecular ordering is required in producing stable molecular glasses, and whether other structural properties, such as layered packings [42], can also play a role in the observed birefringence.

In most molecular systems, it is exceedingly challenging to distinguish the role of orientation vs layering in the observed birefringence. Here, we design a unique molecule, 9-(3,5-di(naphthalen-1-yl)phenyl)anthracene (α,α-A) [inset of Fig. 1(b)] [12,35], to decouple these two effects. The anthracyl substituent introduces steric hindrance to resist rotations around the central benzo ring, allowing α,α-A to retain a nearly isotropic shape. Anthracyl is also an intrinsic fluorescent tag, which can be treated as a linear absorber and emitter, enabling us to apply angle- and polarization-dependent photoluminescence (PL) to directly measure its orientation. Since α,α-A lacks strong

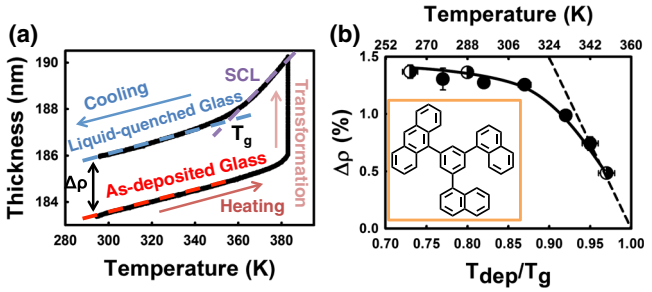

FIG. 1. (a) Thickness vs temperature for α,α-A deposited at $T_{dep} = 0.80$, $T_g = 288$ K. Heating and cooling rates were 1 K/min. Dashed lines are linear fits to SG, liquid-quenched glass, and SCL regimes used to evaluate T_g and relative density $\Delta\rho$. (b) Density difference between the SGs and transformed liquid-quenched glasses, $\Delta\rho$, as a function T_{dep}. Filled symbols were reported in Ref. [35]. Half-filled symbols are obtained in this work. The dashed line is the extrapolated SCL line and the solid line is the guide to the eye. The inset is the molecular structure of α,α-A.

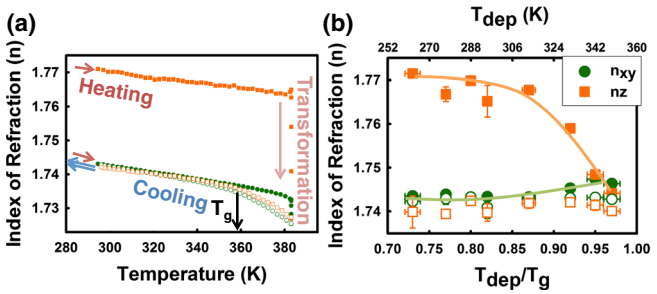

FIG. 2. (a) n_{xy} (green) and n_z (orange) of the same film as shown in Fig. 1(a) as a function of temperature. (b) Calculated n_{xy} (green) and n_z (orange) of as-deposited (filled) and transformed (open) films as a function of T_{dep}. Two individual depositions were carried out at each T_{dep}. All indices were measured at $T = 296$ K and $\lambda = 632.8$ nm. Solid lines are guides to the eye.

intermolecular interactions, and anthracyl exhibits the largest interaction among all substituents [43], anthracyl's orientation is used to infer the overall molecular alignment. Angle-dependent PL has been used in the past to characterize molecular orientation in glasses doped with fluorescent molecules [44]. Polarization-dependent PL [45] and angle- and polarization-dependent Raman scattering [46] have both been applied to carbon nanotubes to characterize the orientation orders, and we adopt a similar experimental setup here.

α,α-A was synthesized and vapor deposited into films of 190 ± 20 nm at various substrate temperatures with a rate of 0.20 ± 0.03 nm/s [$0.73T_g < T_{dep} < 0.97T_g$; see experimental details in Supplemental Material (SM)]. Figure 1(a) shows a measurement of stability of an as-deposited α,α-A film using spectroscopic ellipsometry. Upon heating, the film expands while maintaining its original glassy state until the temperature well exceeds T_g. Isothermal holding at $T_g + 23$ K transforms the glass into SCL. When complete, the SCL is cooled and measures $T_g = 360$ K. The film's density change is evaluated by the thickness change at 296 K. The relative density change as a function of T_{dep} is shown in Fig. 1(b). The dashed line represents the extrapolated equilibrium density of SCL [20,35]. For the deposition rate chosen here, $T_{dep} > 0.95T_g$ produces glasses with densities equal to that of the equilibrium state. Decreasing T_{dep} results in the formation of kinetically trapped states, with densities higher than the liquid-quenched glass, but lower than equilibrium SCL.

Ellipsometry was also used to simultaneously measure the in-plane (n_{xy}) and out-of-plane (n_z) indices of refraction in these transparent SGs in the wavelength range of 600–1600 nm [35]. Figure 2(a) shows the evolution of n_{xy} and n_z at $\lambda = 632.8$ nm during the transformation described in Fig. 1(a). While a large decrease in n_z is observed during transformation, indicating reduced density upon heating, surprisingly little change is measured in n_{xy}. This trend holds true for all SGs in the T_{dep} range in this study (see additional data in SM). When equilibrated to SCL, birefringence disappears (similar values of n_{xy} and n_z). Below T_g, a small positive birefringence emerges, which can be attributed to the stress-optical effect [47–49] due to the mismatch in the expansion coefficients of the glass and the substrate [34,50]. Figure 2(b) shows n_{xy} and n_z of as-deposited SGs and transformed values measured at $T = 296$ K. n_z of SGs strongly depends on T_{dep}, and reaches a plateau value of 1.77 at $T_{dep} = 0.87\,T_g$. However, n_{xy} remains relatively constant at all T_{dep} values and is the same as the n_{xy} of the liquid-quenched glass.

To identify the role of preferential orientational order of molecules in the observed birefringence, angle- and polarization-dependent PL studies were performed on these samples to determine alignment of the anthracyl substituents. The $S0 \leftrightarrow S1$ transition lies in the plane of anthracyl along (9,10) carbon positions [inset of Fig. 3(a)] [51,52]. Samples were rotated between −70° and 70° in 5°

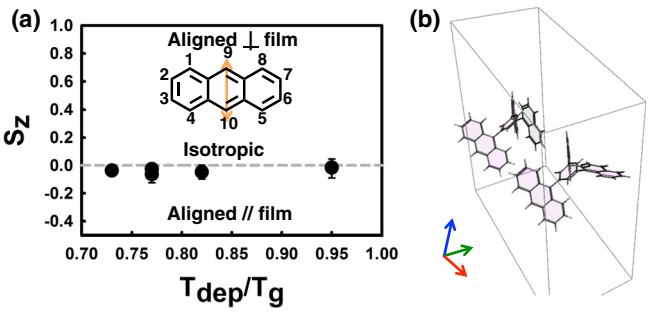

FIG. 3. (a) Orientational nematic order parameter, S_z, vs T_{dep}/T_g as determined from simulated fits to angle- and polarization-dependent PL data of α,α-A films. All samples indicate isotropic orientation of the anthracyl substituents. (b) Single crystal unit cell of α,α-A.

increments. Polarization-resolved PL is measured for the $S1 \rightarrow S0$ transitions with four excitation and emission polarization combinations, I_{pp}, I_{sp}, I_{ps}, and I_{ss}, where the first (second) subscript refers to the incident (collected) polarization (p- or s-polarized light), while the film is rotated about a fixed axis. Two PL intensity ratios, I_{pp}/I_{sp} and I_{ps}/I_{ss}, chosen to cancel instrumental efficiencies and angle-dependent power differences in the collection line, were calculated for each angle over a 15 nm bandwidth about the peak emission of α,α-A for each film (465–480 nm) (SM, PL correction [53]).

PL ratios were analyzed by simulating the angle-dependent PL from α,α-A films as a pressed spherical distribution of linear anthracyl substituents. Each anthracyl was modeled as a linear absorber and emitter with perfect polarization memory, the dependence of the PL emission polarization on the absorbed polarization direction, because the $S0 \leftrightarrow S1$ transitions are parallel. When a collection of these linear molecules is considered, however, the perfect polarization memory restriction may be relaxed due to intermolecular energy transfer. Monte Carlo simulations modeling the angle and polarization dependence of the PL from a collection of these anthracyls in the limit of both full and zero polarization memory were used to replicate the experimental data and extract a nematic order parameter, $S_z = (3\langle\cos^2\theta\rangle - 1)/2$, which describes the orientation angle (θ) of the $S0 \leftrightarrow S1$ transition axis with respect to normal and thus quantifies the alignment of anthracyl substituents in the α,α-A films (SM, Monte Carlo simulation of linear absorbers and emitters). $S_z \in [-0.5, 1]$, where $S_z = -0.5$ ($S_z = 1$) corresponds to the $S0 \leftrightarrow S1$ transition axis aligned parallel (perpendicular) to the film and $S_z = 0$ implies no net alignment along z. The best fit order parameters are shown in Fig. 3(a). Error bars were determined by varying S_z and computing the mean squared error (MSE) of the model, then determining the values of S_z above and below the optimal S_z value that doubles MSE relative to its minimum value. For all T_{dep} values, the best fit for the angle- and polarization-dependent PL data suggests that the orientation of the anthracyl substituents is predominately random (S_z near 0), indicating random orientation of the molecules.

One can reasonably question whether the small birefringence here represents an orientational order too small to be detected by PL. To rule this out, we compare the maximum birefringence in SGs with the density functional theory (DFT) calculated value in crystal unit cell. The estimated birefringence in α,α-A crystal is 0.036, taken as the difference between the index of refraction along the PL measured anthracyl's $S0 \leftrightarrow S1$ transition direction vs that along orthogonal directions (SM, DFT unit cell) [63,64]. $\Delta n = 0.03$, the maximum birefringence measured in SGs, would require a crystalline order. Since DFT is subject to error, an upper bound of $\Delta n = 0.13$ is estimated in anthracene crystals [65], with one principal axis projected to anthracene's $S0 \leftrightarrow S1$ transition axis (SM, comparison with anthracene crystal). $\Delta n = 0.03$ is large compared to that in the most-ordered packing of anthracene and requires 1/4 of the molecules to order. As such, to achieve $\Delta n = 0.03$ in SGs by orientation would require significant ordering of α,α-A molecules.

Furthermore, in PVD glasses with preferential molecular alignments, $T_{dep} < 0.8T_g$ typically yields negative birefringence ($\Delta n = n_z - n_{xy} < 0$) [20,25,26,28,34,66,67]. At low T_{dep} values, long axes of the immobile molecules predominantly orient parallel to the substrate, templating a film with average in-plane orientation [25,28–30]. In contrast, $T_{dep} > 0.8\ T_g$ results in positive birefringence. Such alignment is hypothesized to originate from molecules orienting normal to the film's surface in layers immediately below the free surface during PVD [28,31,40,68]. Since birefringence due to alignment relies on the anisotropic molecular shape, one would expect to measure isotropic orientation, or zero birefringence, in SGs of nearly isotropic molecules, such as α,α-A.

Indeed, PL experiments confirm that α,α-A molecules adopt predominantly isotropic orientation at all T_{dep} values [Fig. 3(a)]. We attribute this phenomenon to the built-in steric hindrance of the molecules that prevent them from assuming a planar geometry, even in their crystal form [Fig. 3(b)]. However, α,α-A SGs are birefringent at all T_{dep} values (Figs. 2 and S4). The value of birefringence remains positive even for SGs deposited at the lowest T_{dep} here ($0.73\ T_g$), ruling out in-plane molecular orientation. To our knowledge, this is the first SG system that retains positive birefringence at low T_{dep}.

The increase in birefringence is almost entirely due to the increasing n_z [Fig. 2(b)]. If birefringence in these samples originates from molecular orientation, increased n_z due to dipole alignment in z direction would be accompanied by decreased index values in the other two directions (n_{xy}), keeping the average n constant. Here, increasing n_z is decoupled form n_{xy}, which remains constant as T_{dep} decreases. Thus, factors other than molecular ordering must be considered for increased birefringence.

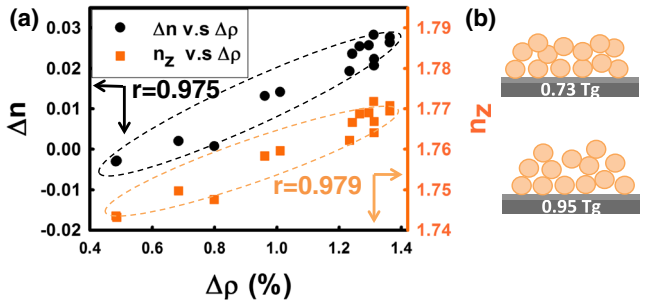

FIG. 4. (a) Correlation of Δn to density change (black) and n_z to density change (orange). Values of all 16 measured samples were reported. (b) Schematic molecular packing in the most ($T_{dep} = 0.73\ T_g$) and least ($T_{dep} = 0.95\ T_g$) anisotropic α,α-A glasses with random orientation.

Figure 4(a) shows that indeed there is a strong correlation between density and n_z ($r = 0.979$), as well as density and birefringence ($r = 0.975$). To understand this trend, we note that in the transparent region, away from the band gap, the polarizability and as such the index of refraction originate from the strength of the induced transition dipoles, and the polarizability can be related to the strength of the local electric field through the Clausius-Mossotti relationship [69]. As the density increases at lower T_{dep} values, the local electric field, and thus the average index of refraction must increase. Furthermore, even with isotropic dipole orientations, anisotropies in packing dimensions alone can lead to birefringence in the material [70]. Consider the extreme limit of a solid crystal with transition dipole moments oriented randomly at every site. Using the relationship between polarizability and transition density, this limit is equivalent to a solid crystal with random site polarizability. If the crystal is cubic, with equal spacings among sites in all three spatial directions, the standard Clausius-Mossoti relationship (which sums up long-range dipole forces) would imply no birefringence. However, Ref. [70] demonstrates how, for the case of asymmetric geometric packing (i.e., with different packing in different spatial directions), the total macroscopic field is different depending on the direction of the applied external fields (and thus leads to birefringence). This birefringence arises because the local field at one lattice site feels long-range effects from the infinitely many other lattice sites, and since those lattice sites have an asymmetric packing, the dipoles in certain directions contribute more to the self-consistent polarization.

This analogy can be extended to disordered systems, with different average intermolecular distances in different directions. Given that n_{xy} is insensitive to T_{dep} values, one must presume that the packing, and therefore the pair correlation function along the xy plane, is also insensitive to the T_{dep} values. Therefore, we hypothesize that the observed birefringence is caused by decreasing of the out-of-plane spacing between the molecules in the z direction to allow the glass to obtain a larger, three-dimensional density (on average).

To rationalize these observations, we consider the nature of the surface-mediated equilibration process. Simulations showed that during deposition, molecules mostly relax in plane, and equilibrate into lower energy states while forming layered structure along the direction normal to the substrate [42]. WAXS experiments on indomethacin SGs [37] observed that the in-plane structure was similar to that of the ordinary glass, with an extra anisotropic peak observed in the out-of-plane direction. Future WAXS or other structural studies on α, α-A can directly measure the pair correlation functions in plane and out of plane to investigate their anisotropic layered packings.

Many properties of SGs resemble those of aged glasses. Specifically, the evolution of density towards equilibrium suggests that the SME process is similar to aging but with a significantly faster rate. Thus, the mobile layer possibly induces a layer with enhanced aging rate beneath, similar to those observed in polymeric glasses [71–75]. As such, the density potentially continues to increase even when molecules are buried below the mobile layer. Since the system is constrained in the xy plane by the substrate, one would expect the increased density due to this additional aging to only affect the intermolecular distance in the z direction. This is consistent with the increased n_z without changes in n_{xy}, which is hard to justify otherwise.

Whether SGs have the same packings as aged ones or are more liquid crystalline in nature is an important question. In particular, the former allows one to gain insight into SCL properties at experimentally inaccessible low temperatures, to address important questions such as avoidance of the Kauzmann crisis [76]. However, previous observations of alignment-induced birefringence seemed to favor the latter scenario. Here we demonstrated the possibility of achieving high-density SG states without orientational order, which can provide important information about the SME process, and the nature of low-energy equilibrium liquids. Furthermore, our study shows that birefringence is not always a sign of molecular alignment in SGs. One must decouple the effect of packing from orientation using other tools.

In summary, we demonstrated that birefringence in stable glass systems may be due to two independent effects, molecular orientation and anisotropic packing dimensions. The observation of birefringence alone is not adequate to conclude oriented packing. More importantly, we illustrated that obtaining high-density glasses does not necessitate preferential orientation of molecules or semicrystalline packing. We hypothesize that birefringence in α,α-A stable glass is because of enhanced aging rates in layers below the mobile surface. The enhanced aging rate combined with substrate constraints can result in differences in the average intermolecular distance in the direction out of plane vs in plane. Such packing anisotropy is also illustrated in the strong correlation between the degree of apparent aging, or increased density with birefringence. The above results inform us on the properties of low-energy glassy systems and the possibility to produce stable glasses that share the same energy landscape as well-aged glasses.

We thank Neil C. Tomson, Wenjie Dou, and Fan Zheng for initializing the simulation, Qingjie Luo and Yi-Chih Lin for liquid phase photoluminescence, Patrick Carroll for x-ray crystallography, and Jeffrey Meth (DuPont), Salvatore Torquato (Princeton), and Abraham Nitzan (UPenn) for helpful discussion. We thank Kim Mullane and Sharan Mehta for collecting 1-Bromo-3-chloro-5-iodobenzene synthesized by undergraduate students in the Chemistry 245 laboratory course. This work was funded by Materials Research Science and Engineering Center (MRSEC) seed Grant from the National Science Foundation (NSF) Grant No. DMR-11-20901 at the University of Pennsylvania (Z. F.), NSF Grant No. DMR-1206270 (J. M. K.), Presidential

Early Career Awards for Scientists and Engineers under (U.S.) Air Force Office of Scientific Research (USAFOSR) Grant No. FA9950-13-1-0157 (J. E. S.), NSF Grant No. CHE-1464744 (P. J. W.), and NSF Grant No. DMREF-1628407 (Z. F. and P. J. W.).

*fakhraai@sas.upenn.edu

[1] M. D. Ediger, C. A. Angell, and S. R. Nagel, J. Phys. Chem. **100**, 13200 (1996).
[2] P. G. Debenedetti and F. H. Stillinger, Nature (London) **410**, 259 (2001).
[3] A. J. Kovacs, J. Polym. Sci. **30**, 131 (1958).
[4] L. C. E. Struik, Polym. Eng. Sci. **17**, 165 (1977).
[5] L. C. E. Struik, *Physical Aging in Amorphous Polymers and other Materials* (Elsevier, Amsterdam, 1978).
[6] I. M. Hodge, Science **267**, 1945 (1995).
[7] M. Utz, P. G. Debenedetti, and F. H. Stillinger, Phys. Rev. Lett. **84**, 1471 (2000).
[8] K. Chen and K. S. Schweizer, Phys. Rev. Lett. **98**, 167802 (2007).
[9] J. Zhao, S. L. Simon, and G. B. McKenna, Nat. Commun. **4**, 1783 (2013).
[10] T. Pérez-Castañeda, R. J. Jiménez-Riobóo, and M. A. Ramos, Phys. Rev. Lett. **112**, 165901 (2014).
[11] S. S. Dalal and M. D. Ediger, J. Phys. Chem. Lett. **3**, 1229 (2012).
[12] T. Liu, K. Cheng, E. Salami, F. Gao, E. Glor, M. Li, P. Walsh, and Z. Fakhraai, Soft Matter **11**, 7558 (2015).
[13] K. L. Kearns, S. F. Swallen, M. D. Ediger, T. Wu, and L. Yu, J. Chem. Phys. **127**, 154702 (2007).
[14] K. L. Kearns, K. R. Whitaker, M. D. Ediger, H. Huth, and C. Schick, J. Chem. Phys. **133**, 014702 (2010).
[15] M. Ahrenberg, Y. Z. Chua, K. R. Whitaker, H. Huth, M. D. Ediger, and C. Schick, J. Chem. Phys. **138** (2013).
[16] S. F. Swallen, K. L. Kearns, M. K. Mapes, Y. S. Kim, R. J. McMahon, M. D. Ediger, T. Wu, L. Yu, and S. Satija, Science **315**, 353 (2007).
[17] K. L. Kearns, S. F. Swallen, M. D. Ediger, T. Wu, Y. Sun, and L. Yu, J. Phys. Chem. B **112**, 4934 (2008).
[18] S. F. Swallen, K. Windsor, R. J. McMahon, M. D. Ediger, and T. E. Mates, J. Phys. Chem. B **114**, 2635 (2010).
[19] K. R. Whitaker, M. Ahrenberg, C. Schick, and M. D. Ediger, J. Chem. Phys. **137** (2012).
[20] S. S. Dalal, Z. Fakhraai, and M. D. Ediger, J. Phys. Chem. B **117**, 15415 (2013).
[21] C. Rodríguez-Tinoco, M. Gonzalez-Silveira, J. Ràfols-Ribé, G. Garcia, and J. Rodríguez-Viejo, J. Non-Cryst. Solids **407**, 256 (2015).
[22] Y. Z. Chua, M. Ahrenberg, M. Tylinski, M. D. Ediger, and C. Schick, J. Chem. Phys. **142**, 054506 (2015).
[23] H.-W. Lin, J. Appl. Phys. **95**, 881 (2004).
[24] D. Yokoyama, A. Sakaguchi, M. Suzuki, and C. Adachi, Appl. Phys. Lett. **93**, 173302 (2008).
[25] D. Yokoyama, A. Sakaguchi, M. Suzuki, and C. Adachi, Org. Electron. **10**, 127 (2009).
[26] D. Yokoyama and C. Adachi, J. Appl. Phys. **107**, 7 (2010).
[27] M. Oh-e, H. Ogata, Y. Fujita, and M. Koden, Appl. Phys. Lett. **102**, 101905 (2013).
[28] S. S. Dalal, D. M. Walters, I. Lyubimov, J. J. de Pablo, and M. D. Ediger, Proc. Natl. Acad. Sci. U.S.A. **112**, 4227 (2015).
[29] J. Gómez, J. Jiang, A. Gujral, C. Huang, L. Yu, and M. D. Ediger, Soft Matter **12**, 2942 (2016).
[30] J. Jiang, D. M. Walters, D. Zhou, and M. D. Ediger, Soft Matter **12**, 3265 (2016).
[31] I. Lyubimov, L. Antony, D. M. Walters, D. Rodney, M. Ediger, and J. J. de Pablo, J. Chem. Phys. **143**, 094502 (2015).
[32] A. Haji-Akbari and P. G. Debenedetti, J. Chem. Phys. **143**, 214501 (2015).
[33] K. L. Kearns, T. Still, G. Fytas, and M. D. Ediger, Adv. Mater. **22**, 39 (2010).
[34] S. S. Dalal, A. Sepulveda, G. K. Pribil, Z. Fakhraai, and M. D. Ediger, J. Chem. Phys. **136**, 204501 (2012).
[35] T. Liu, K. Cheng, E. Salami-Ranjbaran, F. Gao, C. Li, X. Tong, Y.-C. Lin, Y. Zhang, W. Zhang, L. Klinge, P. J. Walsh, and Z. Fakhraai, J. Chem. Phys. **143**, 084506 (2015).
[36] K. J. Dawson, L. Zhu, L. Yu, and M. D. Ediger, J. Phys. Chem. B **115**, 455 (2011).
[37] K. Dawson, L. A. Kopff, L. Zhu, R. J. McMahon, L. Yu, R. Richert, and M. D. Ediger, J. Chem. Phys. **136** (2012).
[38] T. Pérez-Castañeda, C. Rodríguez-Tinoco, J. Rodríguez-Viejo, and M. A. Ramos, Proc. Natl. Acad. Sci. U.S.A. **111**, 11275 (2014).
[39] A. Gujral, K. A. O'Hara, M. F. Toney, M. L. Chabinyc, and M. Ediger, Chem. Mater. **27**, 3341 (2015).
[40] F. Hellman, Appl. Phys. Lett. **64**, 1947 (1994).
[41] H.-B. Yu, Y. Luo, and K. Samwer, Adv. Mater. **25**, 5904 (2013).
[42] S. Singh and J. J. de Pablo, J. Chem. Phys. **134**, 194903 (2011).
[43] C. Gonzalez and E. C. Lim, J. Phys. Chem. A **104**, 2953 (2000).
[44] J. Frischeisen, D. Yokoyama, C. Adachi, and W. Brütting, Appl. Phys. Lett. **96**, 073302 (2010).
[45] O. N. Torrens, D. E. Milkie, H. Y. Ban, M. Zheng, G. B. Onoa, T. D. Gierke, and J. M. Kikkawa, J. Am. Chem. Soc. **129**, 252 (2007).
[46] S. Azoz, A. L. Exarhos, A. Marquez, L. M. Gilbertson, S. Nejati, J. J. Cha, J. B. Zimmerman, J. M. Kikkawa, and L. D. Pfefferle, Langmuir **31**, 1155 (2015).
[47] F. Ay, A. Kocabas, C. Kocabas, A. Aydinli, and S. Agan, J. Appl. Phys. **96**, 7147 (2004).
[48] M. F. Hossain, H. P. Chan, and M. A. Uddin, Appl. Opt. **49**, 403 (2010).
[49] M. K. Szczurowski, T. Martynkien, G. Statkiewicz-Barabach, W. Urbanczyk, L. Khan, and D. J. Webb, Opt. Lett. **35**, 2013 (2010).
[50] J. E. Pye and C. B. Roth, Macromolecules **46**, 9455 (2013).
[51] S. Ateşl and A. Yildiz, J. Chem. Soc., Faraday Trans. 1 **79**, 2853 (1983).
[52] M. Uejima, T. Sato, K. Tanaka, and H. Kaji, Chem. Phys. **430**, 47 (2014).
[53] See Supplemental Material http://link.aps.org/supplemental/10.1103/PhysRevLett.119.095502 for experimental details, calculation of refractive index of α,α-A single crystal in various directions, and discussion of linear absorber and emitter and polarization memory, which includes Refs. [54–62].

[54] J. R. Lakowicz, *Principles of Fluorescence Spectroscopy* (Springer, Boston, 1999), p. 697.
[55] G. Weber, Trans. Faraday Soc. **50**, 552 (1954).
[56] I. Kimura, M. Kagiyama, S. Nomura, and H. Kawai, J. Polym. Sci. A **7**, 709 (1969).
[57] C. R. Desper and I. Kimura, J. Appl. Phys. **38**, 4225 (1967).
[58] V. C. Ballenegger and T. A. Weber, Am. J. Phys. **67**, 599 (1999).
[59] R. W. G. Wyckoff, *The Structure of Benzene Derivatives*, Crystal Structures Vol. 6 (John Wiley and Sons, New York, 1971), pp. 454–456.
[60] G. Vaubel and H. Baessler, Phys. Lett. **27A**, 328 (1968).
[61] H. J. Monkhorst and J. D. Pack, Phys. Rev. B **13**, 5188 (1976).
[62] J. P. Perdew, K. Burke, and M. Ernzerhof, Phys. Rev. Lett. **77**, 3865 (1996).
[63] P. Giannozzi *et al.*, J. Phys. Condens. Matter **21**, 395502 (2009).
[64] Opium pseudopotential generation project, http://opium.sourceforge.net/, 2007.
[65] R. W. Munn, J. R. Nicholson, H. P. Schwob, and D. F. Williams, J. Chem. Phys. **58**, 3828 (1973).
[66] D. Yokoyama, K.-i. Nakayama, T. Otani, and J. Kido, Adv. Mater. **24**, 6368 (2012).
[67] H.-W. Lin, C.-L. Lin, H.-H. Chang, Y.-T. Lin, C.-C. Wu, Y.- M. Chen, R.-T. Chen, Y.-Y. Chien, and K.-T. Wong, J. Appl. Phys. **95**, 881 (2004).
[68] A. Haji-Akbari and P. G. Debenedetti, arXiv:1509.07881.
[69] P. V. Rysselberghe, J. Phys. Chem. **36**, 1152 (1931).
[70] C. Lo, J. T. Wan, and K. Yu, Comput. Phys. Commun. **142**, 453 (2001).
[71] R. D. Priestley, C. J. Ellison, L. J. Broadbelt, and J. M. Torkelson, Science **309**, 456 (2005).
[72] R. D. Priestley, Soft Matter **5**, 919 (2009).
[73] J. E. Pye, K. A. Rohald, E. A. Baker, and C. B. Roth, Macromolecules **43**, 8296 (2010).
[74] A. Shavit, J. F. Douglas, and R. A. Riggleman, J. Chem. Phys. **138**, 12A528 (2013).
[75] A. Shavit and R. A. Riggleman, J. Phys. Chem. B **118**, 9096 (2014).
[76] W. Kauzmann, Chem. Rev. **43**, 219 (1948).